Characterization and corrosion property of nano-rod-like HA on fluoride coating supported on Mg-Zn-Ca alloy

Yashan Feng, Shijie Zhu, Liguo Wang, Lei Chang, Bingbing Yan, Xiaozhe Song, Shaokang Guan[*]

School of Materials Science and Engineering, Zhengzhou University, Zhengzhou, 450002, China

A B S T R A C T

The poor corrosion resistance of biodegradable magnesium alloys is the dominant factor that limits their clinical application. In this study, to deal with this challenge, fluoride coating was prepared on Mg—Zn—Ca alloy as the inner coating and then hydroxyapatite (HA) coating as the outer coating was deposited on fluoride coating by pulse reverse current electrodeposition (PRC-HA/MgF$_2$). As a comparative study, the microstructure and corrosion properties of the composite coating with the outer coating fabricated by traditional constant current electrodeposition (TED-HA/MgF$_2$) were also investigated. Scanning electron microscopy (SEM) images of the coatings show that the morphology of PRC-HA/MgF$_2$ coating is dense and uniform, and presents nano-rod-like structure. Compared with that of TED-HA/MgF$_2$, the corrosion current density of Mg alloy coated with PRC-HA/MgF$_2$ coatings decreases from 5.72×10^{-5} A/cm^2 to 4.32×10^{-7} A/cm^2, and the corrosion resistance increases by almost two orders of magnitude. In immersion tests, samples coated with PRC-HA/MgF$_2$ coating always show the lowest hydrogen evolution amount, and could induce deposition of the hexagonal structure-apatite on the surface rapidly. The results show that the corrosion resistance and the bioactivity of the coatings have been improved by adopting double-pulse current mode in the process of preparing HA on fluoride coating, and the PRC-HA/MgF$_2$ coating is worth of further investigation.

1. Introduction

According to previous in vitro and in vivo research, magnesium alloys are considered as promising bone implant materials for the similarity to sclerotin in mechanical properties and its degradable nature [1—4]. However, early clinical trials report that the rapid degradation rate results in Mg alloy losing mechanical integrity potentially during implantation period [5—7]. Thus, fabricating protective coatings is a promising approach to enhance the corrosion resistance and biological compatibility of Mg alloy [8—11].

Magnesium fluoride (MgF$_2$) coating has been selected as the protective coating due to the non-toxicity, chemically inertness and its simple preparation process [12]. In order to enhance the corrosion resistance and bioactive property of magnesium alloys, many researchers use magnesium fluoride as the intermediate coating and bioactive coating as an outer coating to modify the surface of magnesium [13]. H.R. Bakhsheshi-Rad manufactured HA on magnesium fluoride coating by traditional constant current electrodeposition, and the corrosion resistance is improved as compared with that of separate HA coating [14]. However, during the experimental process, it is found that HA coating prepared on magnesium fluoride coating by TED was loose, uneven and defective. Magnesium fluoride coating has a relatively poor electrical conductivity, which may lead to the uneven distribution of the charges during the preparation process of HA. In addition, concentration polarization in the TED process may aggravate the uneven phenomenon of HA coatings. According to previous research, pulse reverse current (PRC) is capable of generating coating with higher density and stronger anchoring strength compared to constant current electrodeposition [15—17]. Furthermore, if adopting the PRC for depositing HA on fluoride coating, the fluoride coating may be slightly decomposed, and the released F$^-$ would affect the nucleation and growth of HA [18,19]. It is reported that F$^-$ ions doped in hydroxyapatite could provide better degradation

property, better protein adsorption, better cell attachment and improved alkaline phosphatase activity in cell culture [18,20]. Therefore, it is expected that fabricating HA coating on fluoride coating by PRC could improve the biocompatibility and corrosion resistance of the specify Mg-2.1Zn-0.22Ca alloy.

In this study, we succeed in depositing PRC-HA on fluoride coatings supported on Mg-Zn-Ca alloys by PRC electrodeposition. The surface characteristics and the corrosion resistance of PRC-HA/MgF$_2$ coatings are studied. For comparison, TED-HA/MgF$_2$ coatings and bare Mg-Zn-Ca alloy substrate are also evaluated.

2. Experimental

2.1. Preparation of fluoride coatings

As-cast Mg-2.1Zn-0.22Ca alloy prepared in our laboratory was extruded with an extrusion ratio of 25, cylindrical specimens of 5 mm in height and 12 mm in diameter were machined from the extruded material. The samples were grounded and polished with successively finer SiC papers up to 1000 grit, ultrasonically cleaned in acetone and ethylalcohol mixed solution for 10 min. For conversion treatment, the samples were immersed vertically in a plastics bottle containing HF of concentration 40% at room temperature for 24 h. Then the treated samples were rinsed with deionized water and dried in air. During the experiment, appropriate personal protection equipment, including gloves and mask, should be worn while handling the material to avoid the harmful effects of HF.

2.2. Synthesis of Ca–P coatings

Ca–P coating was prepared using the electrochemical workstation (RST5200, KeRui Instruments, Gongyi, China). A graphite plate was used as the anode and the samples coated with the fluoride coating served as the cathode. The electrolyte was prepared by dissolving calcium nitrate (Ca(NO$_3$)$_2$·4H$_2$O, 0.042 mol/L), ammonium dihydrogen phosphat (NH$_4$H$_2$PO$_4$, 0.025 mol/L) and sodium nitrate (NaNO$_3$, 0.1 mol/L) in deionized water. Nitric acid (HNO$_3$) solution and trihydroxymethyl aminomethane ((CH$_2$OH)$_3$CNH$_2$) were used to adjust the pH to 5.0. The electrodeposition was carried out at 80 °C in a water bath for 20 min. PRC parameters for the deposition process was optimized in previous studies in our laboratory [21]. The TED process was carried out in galvanostat mode and the cathodic current density was maintained at 1 mA/cm^2 for 20 min. Magnetic stirring was controlled at 25 rpm to keep the concentration uniform. After deposition, the specimens were rinsed in distilled water, and then dried in air.

2.3. Coating characterization

The crystalline phase of the fluoride coating and composite coatings were identified with X-ray diffractometer (XRD philips 1700X, philips, Netherlands) using Cu Kα1 radiation (at a scan rate of 2°/min). The morphologies of the coatings and the cross-section of the composite coating were examined by scanning electron microscope (SEM Quanta-200, FEI, Netherlands) equipped with EDS (energy dispersive X-ray spectroscopy). The growth morphologies of the Ca-P coating were identified by another scanning electron microscope (SEM JSM-6700F, JEOL, Japan). The functional groups of the coatings were analyzed using a fourier-transformed infrared spectrophotometer (FTIR 5700, Nicolet, America).

2.4. Ion chromatography

In order to investigate the effect of different electrodepositon mode on fabricating HA on fluoride coating, the electrolyte nearby the working electrode was collected after deposition for 10 min and the ion concentration of F$^-$ of the electrolyte was measured with ion mass spectroscopy (ICS1500, DIONEX, America).

2.5. Electrochemical studies

Electrochemical tests were carried out using a classical three electrodes cell with a platinum rod as the auxiliary electrode, a saturated calomel electrode as the reference electrode and the samples as the working electrode. The simulated body fluid (SBF) was prepared according to previous studies [22]. The electrolyte was buffered at pH = 7.4 using tris-hydroxymethyl aminomethane ((HOCH$_2$)$_3$CNH$_2$) and hydrochloric acid (HCl), kept at 37 °C. The sample area exposed to the solution was 1 cm^2. The measurements were carried out at a scan rate of 0.5 mV/s using an electrochemical station and the sample was kept in the solution for 1 h before polarization tests to establish the open circuit potential.

2.6. Immersion test

Different kinds of samples were carefully embedded into silica gel with only one side of 1 cm^2 exposed. Then samples were immersed in 20 ml SBF in sterilized bottle in a water bath at 37 °C for 15 days. For hydrogen evolution test, the record time interval was lengthened with the proceed of immersion test. After immersion, the samples were rinsed with distilled water and dried in vacuum drying oven for 2 h. The morphologies of the Ca-P coating after immersion for 10 days were observed by scanning electron microscope (SEM, Quanta-200).

3. Results and discussion

3.1. Microstructure and composition of the coatings

The SEM image and EDS result of the fluoride coating are shown in Fig. 1. The fluoride coating is uniform and compact, and no microcrack is detected, which plays a very crucial role in the enhancement of corrosion resistance [23–25]. According to the EDS spectra of the fluoride coating in Fig. 1(b), four elements are detected in the coating: magnesium, fluorine, oxygen and a small amount of Au. Au element was intentionally sprayed on the surface of samples before scanning process. O element may originate from the oxide of magnesium generated during the fluorination process. The presence of fluorine element indicates that fluoride coating has been successfully coated on Mg alloy surface.

SEM images of HA on fluoride coating prepared by different power sources are shown in Fig. 2. Because of the concentration polarization, hydrogen evolution and poor conductivity of fluoride coating, the TED-HA/MgF$_2$ coating is uneven. The surface presents to be micro-flake-like structure, and many agglomerated parts appear on the surface with pores in the center. In biological environment, body fluid would infiltrate into the pores and induce fast corrosion of the substrates. The agglomerated parts are comparatively easy to shed off, which may result in inflammation during implantation periods [26]. By contrast, the PRC-HA/MgF$_2$ coating shows compact nano-rod-like structure and covers the fluoride coating surface completely. The diameter of rod-like crystals is ranging from 50 to 80 nm. Compared to flake-like coating, the rod-like coating would provide much better protection to the substrate due to the dense and uniform structure, and it may be more favorable for the deposition of apatite owing to the increased contact area with the surrounding fluid after implantation. Moreover, It is reported that nano-sized HA is more beneficial for bone cell adhesion and proliferation [27]. Fig. 3 shows the corresponding
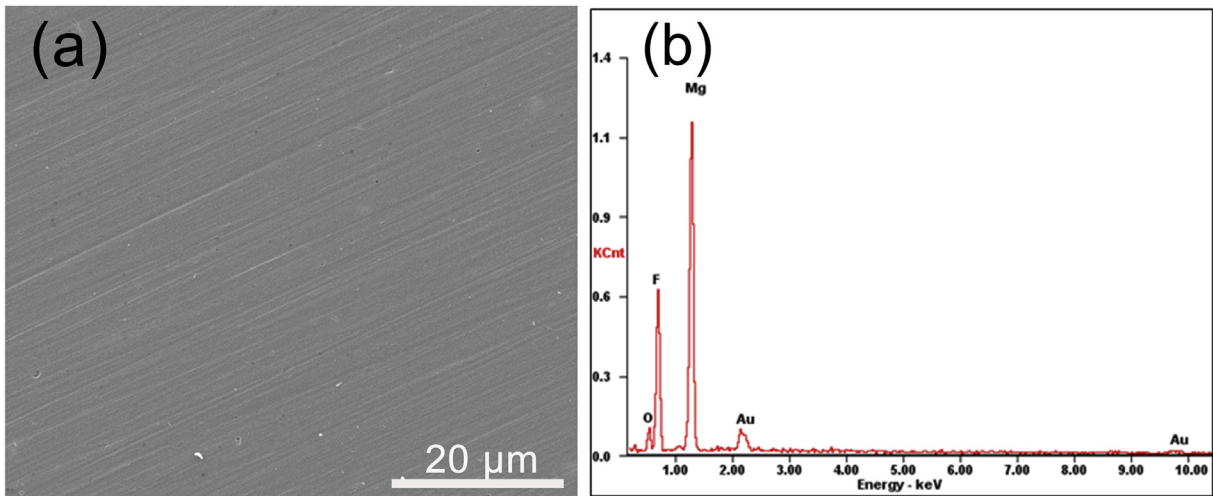
Fig. 1. The morphology and characterization of the fluoride coating: (a) SEM image; (b) EDS result.

EDS results of the coatings. The Ca/P ratio of TED-HA/MgF$_2$ coatings is ranged from 1.21 to 1.29, and the Ca/P ratio of PRC-HA/MgF$_2$ coatings is about 1.50. Both outer coatings are composed of calcium-deficient HA, which may poss excellent biodegradation and induce the precipitation of bone-like apatite after implantation [28–30]. Higher atomic ratio of Ca to P of nano-rod-like HA coating may result from the fluoride coating. In the PRC process, more F$^-$ ions release from fluoride coating and combine with Mg^{2+} ions released from the substrate. In that case, fewer Mg^{2+} ions could occupy the positions of Ca^{2+} ions in the HA lattice. Thus, the calcium content in HA lattice increases relatively [31]. The silicon comes from silica gel, which is used to cover the non-work area of a sample. Na$^+$ ions from NaNO$_3$ in the electrolytes could substitute Ca^{2+} ions in the crystal structure of HA. In Fig. 3(b, a) small amount of F element is detected, which can prove the existence of F$^-$ ions in PRC-HA structure. In the PRC mode, Mg alloys coated with fluoride coating are used as the anode for a few seconds. At this moment, MgF$_2$ coating is slightly decomposed and F$^-$ ions are released from
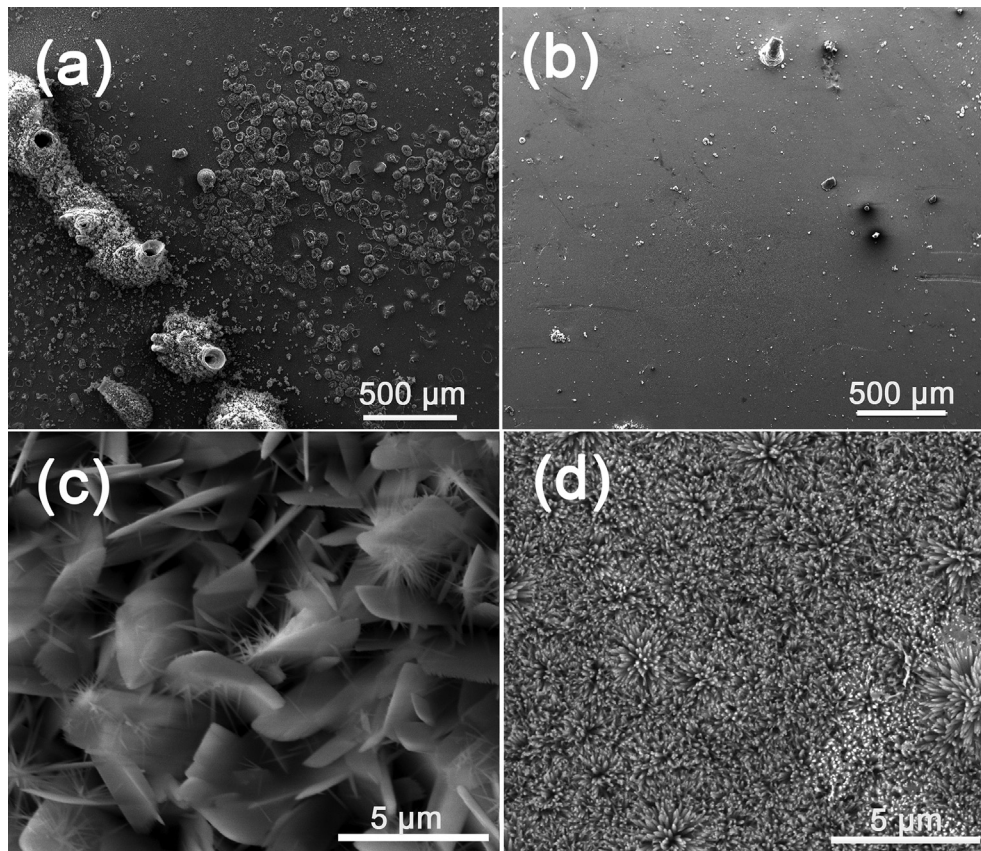

Fig. 2. The SEM images of HA coating on fluoride coating prepared by different power source pattern: (a, c) TED; (b, d) PRC.
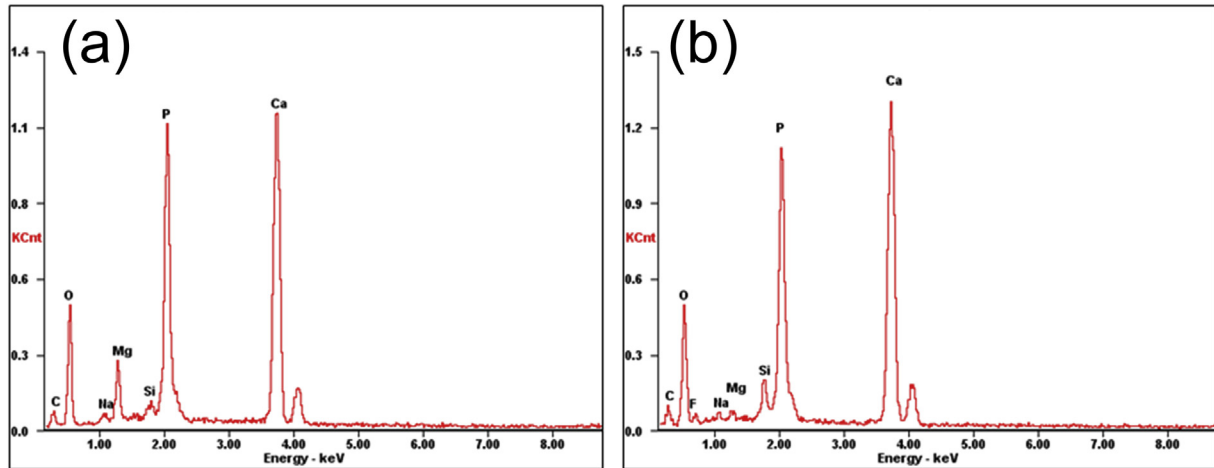
Fig. 3. The EDS results of HA on fluoride coating prepared by different power source pattern: (a) TED; (b) PRC.

the fluoride coating. The released F^- ions was diffused into the electrolyte and act as good nucleation agent, which can enhance the degree of crystallinity, the lattice symmetry and make grain refining. Meanwhile, in the TED mode, Mg-alloys with the fluoride coating are always used as the cathode, and no or fewer F^- ions participate in the nucleation of HA, so the morphology of the Ca-P coating still presents flake-like structure similar to separate HA coating prepared by electrodeposition. Moreover, after PRC deposition experiment, the electrolyte was a little turbid while the electrolyte of the TED was still clean. It may be because F^- ions existed in the electrolyte of PRC combined with Mg^{2+} ions and formed poor solubility MgF_2 suspended in the electrolyte. As it is shown in the ions chromatography results, after deposition for 10 min, F^- ion concentration of the PRC electrolyte near the substrate is 85.196 µg/L and the F^- ion concentration of the TED electrolyte is 18.288 µg/L. It demonstrates that more F^- ions release from the fluoride coating, which affects the nucleation and growth of HA in PRC process.

XRD diffraction patterns of the samples coated with fluoride coating, TED-HA/MgF$_2$ coating and PRC-HA/MgF$_2$ coating are shown in Fig. 4. As is shown in curve A, the XRD peak appeared at 40.4° is corresponding to the crystal plane of tetragonal (110),

which proves the existence of MgF_2 (JCPDS No. 70-2269). Oxygen detected in EDS originates from hydroxides of Mg, because OH^- could replace some F^- ions in MgF_2 structure [32]. The fluoride coating is mainly composed of MgF_2 and a small amount of $Mg(OH)_2$, and the existence of $Mg(OH)_2$ can reduce the ratio of F to Mg as expected from stoichiometric MgF_2. The quantity of $Mg(OH)_2$ may be too little to be detected by XRD. The peaks from both composite coatings match well with the HA pattern (JCPDS No. 09-0432). It is apparent that the peak at 25.8° of PRC-HA/MgF$_2$ XRD pattern which is related to the (002) plane of HA is higher than that of TED-HA/MgF$_2$ coating, suggesting the nano rod-like crystal preferred to be oriented along the c-axis [001] direction [33]. In Fig. 5, FT-IR is used to identify the functional group of the two kinds of coatings. As it is shown that the functional group of the PRC-HA/MgF$_2$ coating is similar with that of TED-HA/MgF$_2$ coating. The vibrational wide bands of 3434 cm^{-1} can be confirmed as the typical peak of OH^- [31]. The absorption peaks at 563 cm^{-1}, 603 cm^{-1}, 1030 cm^{-1} prove the existence of PO_4^{3-}. The band of CO_3^{2-} at 862 cm^{-1} is due to CO_2, which is dissolved in the electrolyte and substitute the positions of PO_4^{3-} in the HA structure. The wide band between 1600 cm^{-1} and 1700 cm^{-1} was caused by H_2O included in the sample.
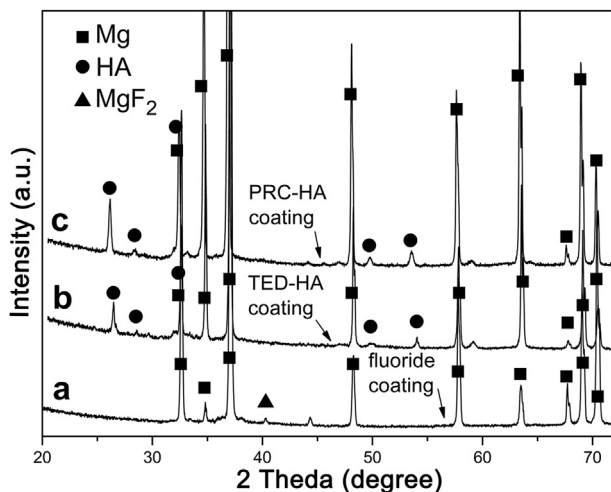

Fig. 4. XRD patterns of different coatings: (a) fluoride coating, (b) TED-HA/MgF$_2$ coating and (c) PRC-HA/MgF$_2$ coating.
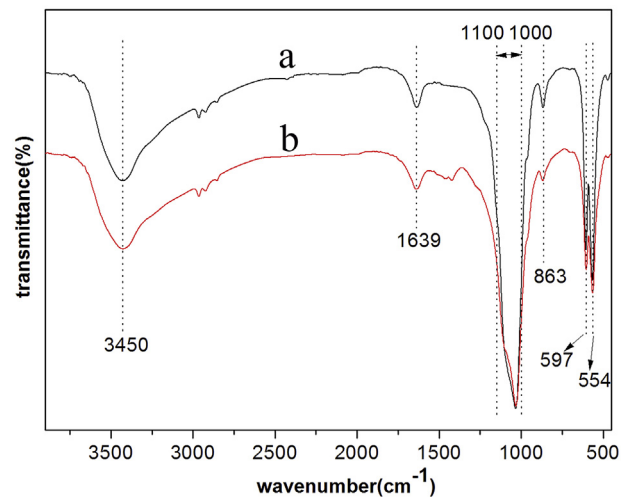

Fig. 5. FTIR spectrum of different coatings: (a) TED-HA/MgF$_2$ and (b) PRC-HA/MgF$_2$ coating.

Fig. 6. The cross-section image of (a) PRC-HA/MgF$_2$ and (b) TED-HA/MgF$_2$ composite coating on Mg-Zn-Ca alloy.

The cross-section photographs of the PRC-HA/MgF$_2$ and TED-HA/MgF$_2$ coating are shown in Fig. 6. In Fig. 6 (a), the thickness of fluoride coating is about 1.2 μm, and the thickness of HA coating is about 1.5 μm. The fluoride coating combines with the Mg alloy substrate and the HA coating tightly, and no visible cracks are observed on the two interfaces. Compared with that of PRC-HA/MgF$_2$, both the thickness of fluoride coating and HA coating of TED-HA/MgF$_2$ are slightly thicker. In the electrodeposition process, MgF$_2$ coating is slightly decomposed when Mg alloys coated with fluoride coating are used as the anode, thus the thickness of the fluoride coating was decreased. In addition, F$^-$ ions can change the lattice parameters of HA and decrease the crystalline sizes, therefore, the thickness of outer HA coating of PRC-HA/MgF$_2$ was also decreased.

The growth steps of flake-like HA coating have been studied [21]. The morphologies of PRC-HA/MgF$_2$ coating in different deposition periods are shown in Fig. 7. It is apparent that the
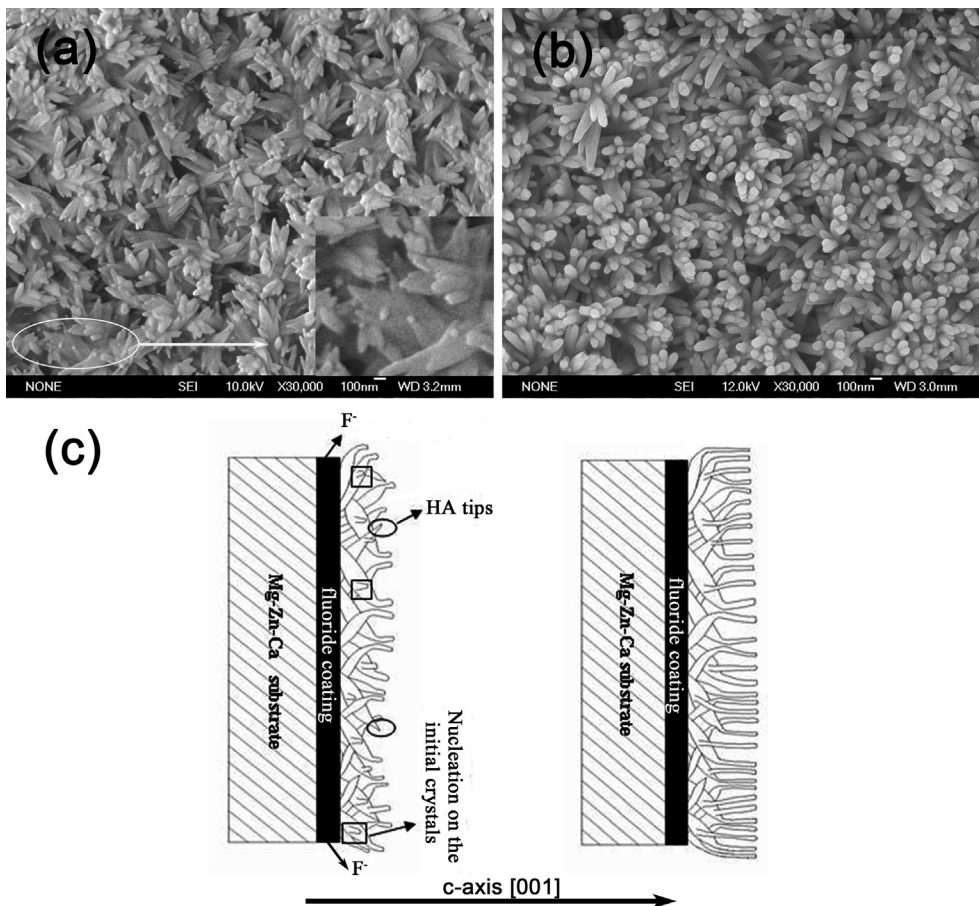

Fig. 7. SEM images of the PRC-HA/MgF$_2$ coating after deposition for (a) 5 min, (b) 10 min and (c) the Schematic drawing of coating growth.

Table 1
Values from the polarization curve of different samples in SBF.

Samples	I_{corr} (A/cm^2)	E_{corr}(V)	R_p (Ω)
Substrate	3.23×10^{-4}	−1.68	1.11×10^2
TED-HA/MgF$_2$ coating	5.81×10^{-5}	−1.60	7.36×10^2
PRC-HA/MgF$_2$ coating	7.84×10^{-7}	−1.53	3.70×10^4

surface is completely covered by bamboo leaf-like crystals after deposition for 5 min and the crystals present a random orientation to the substrate. However, after deposition for 10 min, the morphology changes into typical nano rod-like crystals, and relatively grows along the c-axis. The formation mechanism of the rod-like HA is mainly as follows: in the initial period of the electrochemical deposition, very small amounts of F⁻ ions existed in the electrolytes, which could not effectively influence the nucleation and growth of HA. As the electrochemical deposition proceeds, the more time the substrate works as the anode, the more F⁻ ions are released from the fluoride coating. Thus a large number of F⁻ ions in the electrolytes alternatively occupy the hydroxyl site in the α-axis of HA lattice and make the α-axis dimension contract owing to the smaller size of F⁻ ions [31]. Therefore, HA crystals grow along the concentration gradient of the electrolyte. Additionally, owing to the influence of F⁻ ions, the rod-like crystals could nucleate on the initial bamboo leaf-like crystals and relatively oriented along the c-axis (Fig. 7(a)). Fig. 7 (c) simply shows the schematic drawing of coating growth.

3.2. Corrosion properties

3.2.1. Electrochemical test and hydrogen evolution test

Electrochemical test is a general method to evaluate the corrosion resistance of a sample. Fig. 8 (left) shows typical polarization curves of different types of samples in SBF. Corrosion potential ($Ecorr$), corrosion current density ($Icorr$) and corrosion resistance (Rp) are summarized in Table 1. $Ecorr$ and $Icorr$ are derived directly from the polarization curves and Rp is calculated according to the reported equation [34]:

$$R_p = \frac{b_a b_c}{2.303 i_{corr}(b_a + b_c)} \tag{1}$$

Research indicates that the corrosion resistance of a sample with coating is determined by its corrosion current density and resistance [35]. Compared with the TED-HA/MgF$_2$ coating, the nano-rod-like coating effectively improves the corrosion resistance of the Mg-Zn-Ca alloy, with the corrosion current density decreases from 5.81×10^{-5} to 7.84×10^{-7} A/cm^2 and the resistance is improved by nearly two orders of magnitude. As is shown in Fig. 1(a), TED-HA/MgF$_2$ coating is loose and defective. In biological environment, body fluid may seep into the cracks and pores of TED-HA/MgF$_2$ surface and corrode the substrate. Cracks on the surface would propagate under the stress and lead to coating shedding from the substrate, ultimately, accelerates the corrosion of the substrate. Meanwhile, as compared to TED-HA/MgF$_2$, the surface of PRC-HA/MgF$_2$ coating is compact and uniform, which may provide better protection for the substrate, thus inhibiting corrosive ions from entering into the inner substrate.

The hydrogen evolution results of different specimens in SBF solution for a period of 15 days are shown in Fig. 8 (right). The volume of H$_2$ released from the magnesium substrate increases rapidly with the extension of immersion time. Compared with that of substrate, the released rate of H$_2$ volume of coated samples seems to be constant and less. Compared with TED-HA/MgF$_2$ coated samples, the PRC-HA/MgF$_2$ coated samples perform better and always show the lowest hydrogen evolution amount. By approximate calculation, the corrosion rates of the substrate, TED-HA/MgF$_2$ coated samples and PRC-HA/MgF$_2$ coated samples are 8.97 mm/y, 2.21 mm/y, and 0.96 mm/y, respectively. The evolved H$_2$ from the samples coated with PRC-HA/MgF$_2$ seems to be tolerated by the human body [36]. The hydrogen evolution results indicate that PRC-HA/MgF$_2$ could effectively prevent the substrate from rapid corrosion.

3.2.2. Immersion test

Fig. 9 shows SEM images of TED-HA/MgF$_2$ and PRC-HA/MgF$_2$ coatings immersed in SBF for 10 days. The samples coated with TED-HA/MgF$_2$ have been corroded seriously, leaving cracks and visible bare Mg alloy part on the surface, while the PRC-HA/MgF$_2$ coating retains integrity. In Fig. 9(a), aggregation phenomenon of TED composite coating (Fig. 2(a)) is not observed after 10 days immersion, and apparently, the bare Mg alloys part (Fig. 9(a)) may be covered by the aggregation part before immersion test. The poor
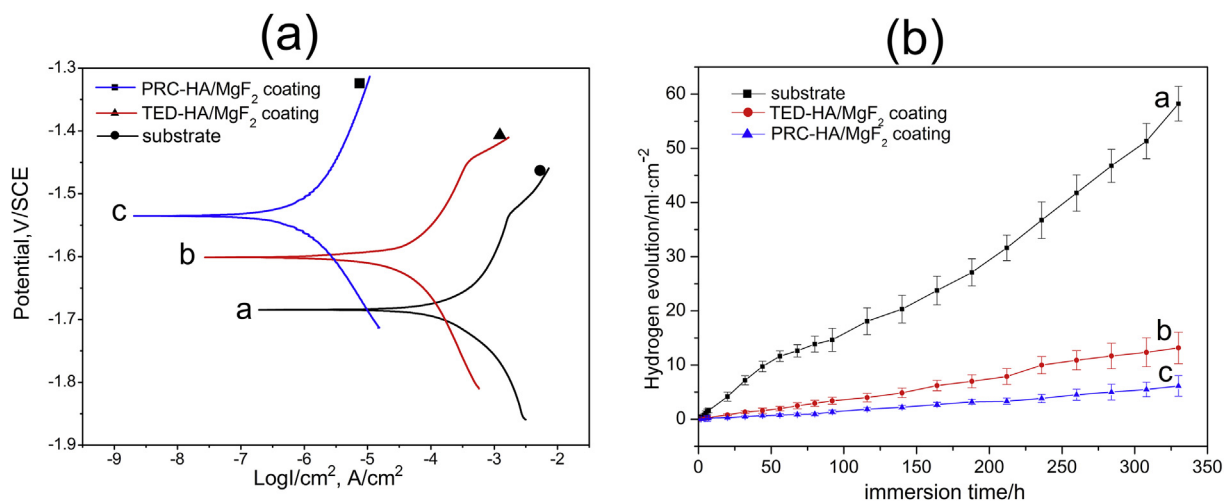
Fig. 8. Polarization curves (left) and hydrogen evolution test (right) of different coatings: (a) as-extruded Mg alloy, (b) TED-HA/MgF$_2$ coating and (c) PRC-HA/MgF$_2$ coating in SBF.
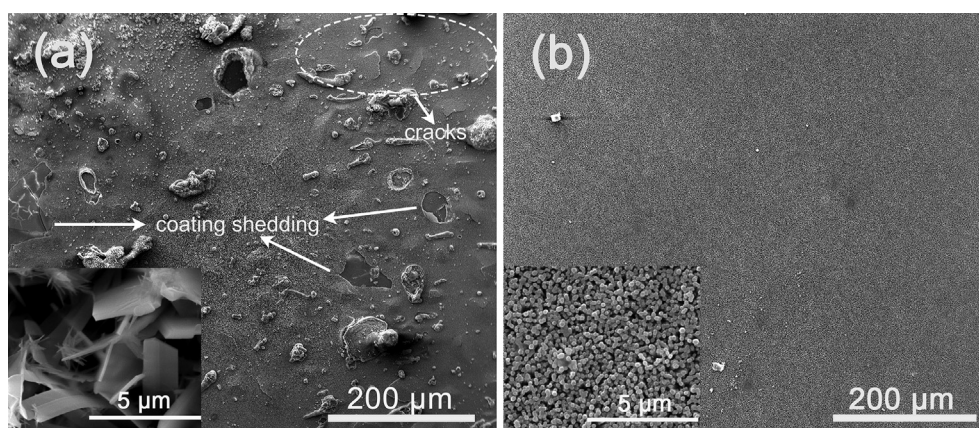
Fig. 9. SEM photographs of (a) TED-HA/MgF$_2$ coating and (b) PRC-HA/Mg coating immersed in SBF for 10 days.

bonding strength and loose structure both result in the aggregation parts peeling off the substrate during the immersion process. In Fig. 9 (b), the PRC-HA/MgF$_2$ coating presents hexagonal structure, which is slightly different from the coating structure before immersion test, but is similar to typical HA structure. It means that PRC-HA/MgF$_2$ coating could absorb Ca^{2+}, PO$_4^{3-}$ from SBF solution rapidly, which can form hexagonal structure-apatite on the surface. According to the photographs, the hexagonal structure-apatite seems to in-situ grow on the top of nano-rod-like HA. It can be attributed to the effect of nano-sized HA, which highly increases the area of interface between PRC-HA structure and SBF, thereby highly enhanced the absorption of Ca^{2+}, PO$_4^{3-}$ in SBF solution. Meanwhile, no visible precipitates appears on TED-HA/MgF$_2$ surface after immersion. That is because the submicron scale coating provides fewer interface for the deposition of apitite compared with the nano scale coating. In addition, previous research has demonstrated that the large amount of Mg^{2+} could restrain the precipitation of apitite [36−38], which provides evidence that TED-HA/MgF$_2$ coated samples have suffered serious corrosion during the immersion period.

4. Conclusions

In this work, HA coating is successfully prepared by PRC on fluoride coating supported on Mg−Zn−Ca alloys and the composition, microstructure and corrosion resistance properties of PRC-HA/MgF$_2$ coatings are evaluated. Compared with the TED-HA/MgF$_2$ coating, PRC-HA/MgF$_2$ coating was dense and uniform and the surface presents nano-rod-like structure with the rod diameter ranging from 50 nm to 80 nm. The nano-rod-like coating enhances the corrosion resistance of the as-extruded Mg alloy, and the corrosion current density decreases by nearly two orders of magnitude. The results of immersion tests indicate that the PRC-HA/MgF$_2$ coating presents better biological activity and higher corrosion resistance. Thus, compared with TED-HA/MgF$_2$ coating, the PRC-HA/MgF$_2$ composite coating has greater potential to be used as biological materials.

Acknowledgement

References

[1] M.P. Staiger, A.M. Pietak, J. Huadmai, G. Dias, Magnesium and its alloys as orthopedic biomaterials: a review, Biomaterials 27 (2006) 1728−1734.

[2] R.C. Zeng, C.L. Yue, K. Jiang, R. Liu, B.D. Zhao, Y.F. Zheng, In vitro corrosion and cytocompatibility of a microarc oxidation coating and poly(L-lactic acid) composite coating on Mg-1Li-1Ca alloy for orthopaedic implants, ACS Appl. Mater. Inter 8 (2016) 10014−10028.

[3] L.J. Liu, P.P Li, Y.H. Zou, K.J. Luo, F. Zhang, R.C. Zeng, S.Q. Li, In vitro corrosion of as-extruded Mg-Ca alloys-The influence of Ca concentration, Corros. Sci. 96 (2015) 23−31.

[4] J. Wang, L.M. Liu, Y.F. Wu, M.F. Maitz, Z.H. Wang, Y. Koo, A.S. Zhao, Y. Yun, Ex vivo blood vessel bioreactor for analysis of the biodegradation of magnesium stent models with and without vessel wall integration, Acta. Mater 50 (2017) 546−555.

[5] F. Witte, J. Fischer, J. Nellesen, H.A. Crostack, V. Kaese, A. Pisch, F. Beckmann, et al., In vitro and in vivo corrosion measurements of magnesium alloys, Biomaterials 27 (2006) 1013−1018.

[6] H. Inoue, K. Sugahara, A. Yamamoto, H. Tsubakino, Corrosion rate of magnesium and its alloys in buffered chloride solutions, Corros. Sci. 44 (2002) 603−610.

[7] H. Kuwahara, N. Mazaki, M. Mabuchi, C. Wein, T. Aizawa, Behavior of magnesium in Hank's solution aimed to trabecular pattern of natural bone, Mater. Sci. Forum 419 (2003) 1007−1012.

[8] L.Y. Cui, S.D. Gao, P.P. Li, R.C. Zeng, F. Zhang, S.Q. Li, E.H. Han, Corrosion resistance of a self-healing micro-arc oxidation/polymethyltrimethoxysilane composite coating on magnesium alloy AZ31, Corros. Sci. 118 (2017) 84−95.

[9] L.Y. Cui, R.C. Zeng, S.K. Guan, W.C. Qi, F. Zhang, S.Q. Li, E.H. Han, Degradation mechanism of micro-arc oxidation coatings on biodegradable Mg-Ca alloys-The influence of porosity, J. Alloy. Compd. 695 (2017) 2464−2476.

[10] L.J. Liu, P.P. Li, Y.H. Zou, K.J. Luo, F. Zhang, R.C. Zeng, S.Q. Li, In vitro corrosion and antibacterial performance of polysiloxane and poly(acrylic acid)/gentamicin sulfate composite coatings on AZ31 alloy, Surf. Coat. Tech. 291 (2016) 7−14.

[11] L.Y. Cui, R.C. Zeng, X.X. Zhu, T.T. Pang, S.Q. Li, F. Zhang, Corrosion resistance of biodegradable polymeric layer-by-layer coatings on magnesium alloy AZ31, Front. Mater. Sci. China 10 (2016) 134−146.

[12] K. Chiu, M. Wong, F. Cheng, H. Man, Characterization and corrosion studies of fluoride conversion coating on degradable Mg implants, Sur. Coat. Tech. 202 (2007) 590−598.

[13] Xiaoli, Zhen, Zhen, Jing, Tingfei, Yudong, Zheng, et al., Multifunctional MgF$_2$/polydopamine coating on Mg alloy for vascular stent application, J. Mater. Sci. Technol. 31 (2015) 733−743.

[14] H.R. Bakhsheshi-Rad, M.H. Idris, M.R. Abdul-Kadir, Synthesis and in vitro degradation evaluation of the nano-HA/MgF$_2$ and DCPD/MgF$_2$ composite coating on biodegradable Mg-Ca-Zn alloy, Sur. Coat. Tech. 222 (2013) 79−89.

[15] M.S. Chandrasekar, M. Pushpavanam, Pulse and pulse reverse plating-Conceptual, advantages and applications, Electrochim. Acta 53 (2008) 3313−3322.

[16] P. Peng, S. Kumar, N.H. Voelcker, E. Szili, R.S.C. Smart, H.J. Griesser, Thin calcium phosphate coatings on titanium by electrochemical deposition in modified simulated body fluid, J. Biomed. Mater. Res. A 76 (2006) 347−355.

[17] S. Lin, R.Z. Legeros, J.P. Legeros, Adherent octacalciumphosphate coating on titanium alloy using modulated electrochemical deposition method, J. Biomed. Mater. Res. A 66 (2003) 819−828.

[18] J. Wang, Y. Chao, Q. Wan, Z. Zhu, H. Yu, Fluoridated hydroxyapatite coatings on titanium obtained by electrochemical deposition, Acta Biomater. 5 (2009) 1798−1807.

[19] E.C. Meng, S.K. Guan, H.X. Wang, L.G. Wang, S.J. Zhu, J.H. Hu, C.X. Ren, et al., Effect of electrodeposition modes on surface characteristics and corrosion

properties of fluorine-doped hydroxyapatite coatings on Mg-Zn-Ca alloy, Appl. Surf. Sci. 257 (2011) 4811–4816.

[20] J. Li, Y. Song, S. Zhang, C. Zhao, F. Zhang, X. Zhang, L. Cao, et al., In vitro responses of human bone marrow stromal cells to a fluoridated hydroxyapatite coated biodegradable Mg-Zn alloy, Biomaterials 31 (2010) 5782–5788.

[21] H.X. Wang, S.K. Guan, X. Wang, C.X. Ren, L.G. Wang, In vitro degradation and mechanical integrity of Mg-Zn-Ca alloy coated with Ca-deficient hydroxyapatite by the pulse electrodeposition process, Acta Biomater. 6 (2009) 1743–1748.

[22] T. Kokubo, H. Takadama, How useful is SBF in predicting in vivo bone bioactivity? Biomaterials 27 (2006) 2907–2915.

[23] Y.Q. Wang, M.Y. Zheng, K. Wu, Microarc oxidation coating formed on SiCw/AZ91 magnesium matrix composite and its corrosion resistance, Mater. Lett. 59 (2005) 1727–1731.

[24] X.N. Gu, W.Y. Zheng, Y. Cheng, Y.F. Zheng, A study on alkaline heat treated Mg-Ca alloy for the control of the biocorrosion rate, Acta Biomater. 5 (2009) 2790–2799.

[25] R.C. Zeng, L. Sun, Y.F. Zheng, H.Z. Cui, E.H. Han, Corrosion and characterisation of dual phase Mg-Li-Ca alloy in Hank's solution: the influence of micro-structural features, Corros. Sci. 79 (2014) 69–82.

[26] J.J. Callaghan, S.H. Dysart, C.G. Savory, The uncemented porous-coated anatomic total hip prosthesis. Two-year results of a prospective consecutive series, J. Bone & Jt. Surg. Am. 70 (1988) 337–346.

[27] Y.P. Lu, Y.M. Chen, S.T. Li, J.H. Wang, Surface nanocrystallization of hydroxy-apatite coating, Acta Biomater. 4 (2008) 1865–1872.

[28] N. Dumelie, H. Benhayoune, D. Richard, D. Laurent-Maquin, G. Balossier, In vitro precipitation of electrodeposited calcium-deficient hydroxyapatite coatings on Ti6Al4V substrate, Mater. Charact. 59 (2008) 129–133.

[29] M.M. Monteiro, N.C.C.D. Rocha, A.M. Rossi, G.D.A. Soares, Dissolution properties of calcium phosphate granules with different compositions in simulated body fluid, J. Biomed. Mater. Res. A 65 (2003) 299–305.

[30] S.V. Dorozhkin, A review on the dissolution models of calcium apatites, Prog. Cryst. Growth. Ch 44 (2002) 45–61.

[31] S. Chen, S. Guan, S. Hou, L. Wang, S. Zhu, J. Wang, W. Li, Characterization and corrosion properties of Ti-O/HA composite coatings on Mg-Zn alloy, Surf. Interface Anal. 43 (2011) 1575–1580.

[32] S. Verdier, N.V.D. Laak, S. Delalande, The surface reactivity of a magnesium-aluminium alloy in acidic fluoride solutions studied by electrochemical techniques and XPS, Aool. Surf. Sci. 235 (2004) 513–524.

[33] E.A.D. Santos, M.S. Moldovan, L. Jacomine, M. Mateescu, J. Werckmann, K. Anselme, P. Mille, et al., Oriented hydroxyapatite single crystals produced by the electrodeposition method, Mat. Sci. Eng. B 169 (2010) 138–144.

[34] M. Stern, A.L. Geary, Electrochemical polarization I. A theoretical analysis of the shape of polarization curves, J. Electrochem. Soc. 104 (1957) 56.

[35] P. Su, X. Wu, Y. Guo, Z. Jiang, Effects of cathode current density on structure and corrosion resistance of plasma electrolytic oxidation coatings formed on ZK60 Mg alloy, J. Alloy. Compd. 475 (2009) 773–777.

[36] F. Witte, J. Fischer, J. Nellesen, C. Vogt, J. Vogt, T. Donath, F. Beckmann, In vivo corrosion and corrosion protection of magnesium alloy LAE442, Acta Biomater. 6 (2010) 1792–1799.

[37] K.S. Tenhuisen, P.W. Brown, Effects of magnesium on the formation of calcium-deficient hydroxyapatite from $CaHPO_4.2H_2O$ and $Ca_4(PO_4)_2O$, J. Biomed. Mater. Res. 36 (1997) 306–314.

[38] L.Y. Cui, Y. Hua, R.C. Zeng, Y.X. Yang, D.D. Sun, S.Q. Li, F. Zhang, E.H. Han, New insights into the effect of Tris-HCl and Tris on corrosion of magnesium alloy in presence of bicarbonate, sulfate, hydrogen phosphate and dihydrogen phosphate ions, J. Mater. Sci. Technol. (2017), http://dx.doi.org/10.1016/j.jmst.2017.01.005.